

## Particle acceleration and magnetic field amplification in hotspots of FR II galaxies: The case study 4C74.26

A.T. Araudo<sup>1</sup>, A.R. Bell<sup>2</sup>, K. Blundell<sup>1</sup>

<sup>1</sup>*University of Oxford, Astrophysics, Keble Road, Oxford OX1 3RH, UK*

<sup>2</sup>*University of Oxford, Clarendon Laboratory, Parks Road, Oxford OX1 3PU, UK*

**Abstract.** It has been suggested that relativistic shocks in extragalactic sources may accelerate the most energetic cosmic rays. However, recent theoretical advances indicating that relativistic shocks are probably unable to accelerate particles to energies much larger than a PeV cast doubt on this. In the present contribution we model the radio to X-ray emission in the southern hotspot of the quasar 4C74.26. The synchrotron radio emission is resolved near the shock with the MERLIN radio-interferometer, and the rapid decay of this emission behind the shock is interpreted as the decay of the downstream magnetic field as expected for small scale turbulence. If our result is confirmed by analyses of other radiogalaxies, it provides firm observational evidence that relativistic shocks at the termination region of powerful jets in FR II radiogalaxies do not accelerate ultra high energy cosmic rays.

### 1. Introduction

Radiogalaxies are the subclass of Active Galactic Nuclei (AGN) where jets are clearly detected at radio frequencies, which in turn are classified in type I and II Faranoff-Riley (FR) galaxies. Hotspots are usually detected at the jet termination region of FR II radiogalaxies. These bright radio synchrotron knots have a size  $\sim 1 - 10$  kpc and are embedded in larger lobes of shocked plasma. The location of the hotspot is coincident with the downstream region of the jet reverse shock, where particles accelerated by the latter emit non-thermal radiation.

Diffusive shock acceleration (DSA) is a well established mechanism to accelerate particles in astrophysical sources where shock waves are present (Bell 1978a,b). Particles diffuse back and forth across the shock and gain energy in each crossing. Therefore, long times are required to accelerate the most energetic cosmic rays unless the magnetic field around the shock is amplified. The amplified turbulent field scatters particles rapidly so that they cross the shock more frequently achieving a higher energy in the available time. The state-of-the-art of DSA in the hotspots of FR II radiogalaxies is a phenomenological picture where the acceleration process finishes when particles start to radiate their energy or when they can escape from the source, i.e. the energy gained is sufficient for the Larmor radius to exceed the size of the acceleration region (Meisenheimer et al. 1989). Assuming that the magnetic field persists over long distances downstream of the shock, the distribution of non-thermal emitting electrons is a broken power-law where the break frequency is determined by a competition

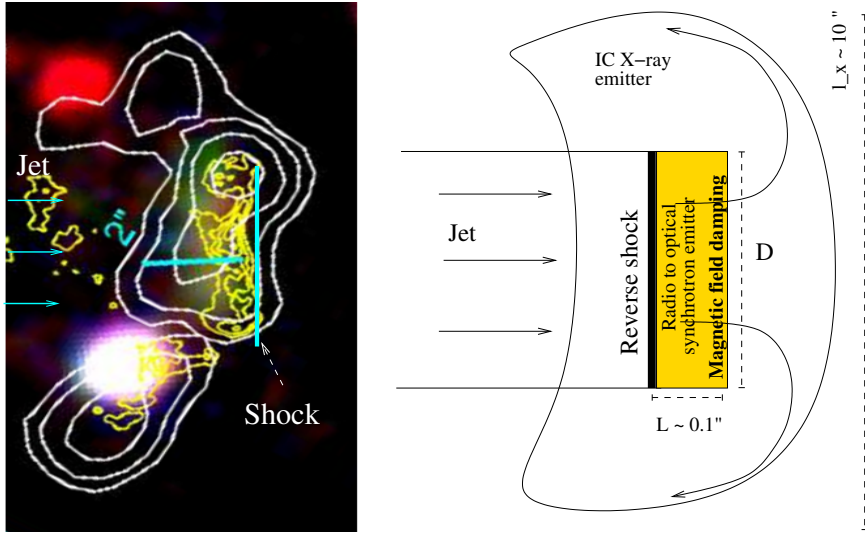


Figure 1. *Left:* Southern arc adapted from Erlund et al. (2010). *Right:* Sketch of the jet termination region (as seen at  $\theta_j = 90^\circ$ ). Particles are accelerated at the reverse shock and radiate in the shock downstream region.

between synchrotron losses and adiabatic expansion (e.g. Brunetti et al. 2003). We will see however that the magnetic field must be highly discrete to explain the very thin radio emission in the southern hotspot of the quasar 4C74.26 (Araudo et al. 2015).

## 2. The case study 4C74.26: the southern hotspot

The FR II radiogalaxy 4C74.26 is located at redshift  $z = 0.104$  ( $\sim 0.5$  Gpc from Earth)<sup>1</sup>. This source is the largest known radio quasar, with a projected linear size of 1.1 Mpc and it has a one-sided jet. Two X-ray sources have been detected with the *Chandra* satellite in the termination region of the South jet (Erlund et al. 2007). The highest X-ray source is called the “X-ray peak” and has no counterpart at other frequencies. On the other hand, the southern X-ray source is coincident with a radio, IR and optical source (Erlund et al. 2010). In the present contribution we focus on this multiwavelength hotspot and assume that this is the jet termination region.

The hotspot X-ray specific luminosity is  $L_x \sim 7.9 \times 10^{40}$  erg s<sup>-1</sup> at frequency  $\nu_x = 2.4 \times 10^{17}$  Hz (2 keV). The shape of this emission is arc-like with a characteristic size  $l_x \sim 10''$ , and encloses a compact radio source, also arc-like and called the “southern arc”, as we show in Figure 1 (left). Compact radio emission from the southern arc was detected with the MERLIN high resolution interferometer

<sup>1</sup>Throughout the paper we use cgs units and the cosmology  $H_0 = 71$  km s<sup>-1</sup> Mpc<sup>-1</sup>,  $\Omega_0 = 1$  and  $\Lambda_0 = 0.73$ . One arcsecond represents 1.887 kpc on the plane of the sky at  $z = 0.104$ .

at a frequency  $\nu_r = 1.66$  GHz with specific luminosity  $L_r \sim 1.9 \times 10^{40}$  erg s $^{-1}$ . This emission is located in a region of width  $l_r < 1''$  on the plane of the sky. In addition, faint and diffuse radiation was detected at IR ( $\nu_{ir} = 1.36 \times 10^{14}$  Hz) and optical ( $\nu_{opt} = 6.3 \times 10^{14}$  Hz) bands, and located in a region of width  $\gtrsim l_r$ . However, there is a linear structure in both bands that traces the brightest edge of the MERLIN radio emission, and seems to be cupped within it.

The measured radio-to-IR spectral index is  $\alpha = 0.75$ , typical of synchrotron radiation, and the steep spectrum between IR and optical indicates that the turnover of the emission is at  $\nu_{ir} \leq \nu_c \leq \nu_{opt}$  (see Fig. 13 in Erlund et al. 2010). Therefore, the southern arc X-ray emission is not synchrotron<sup>2</sup>.

## 2.1. Inverse Compton X-ray emission

The X-ray emission from hotspots is usually explained as synchrotron self Compton (SSC) or up-scattering of Cosmic Microwave Background (CMB) photons (e.g. Hardcastle et al. 2004, Werner et al. 2012). In the case of the southern arc in 4C74.26, SSC is disfavoured because 1) there is an off-set between the peak of the X-ray and radio emission, and 2) the energy density of synchrotron photons is  $8 \times 10^{-15}$  erg cm $^{-3}$ , much smaller than the energy density of CMB photons  $U_{cmb} = 6 \times 10^{-13}$  erg cm $^{-3}$  (Erlund et al. 2010). Therefore, we consider that the X-ray emission from the southern arc is produced by inverse Compton (IC) scattering of CMB radiation.

CMB photons with energy  $E_{cmb} \sim 7 \times 10^{-4}$  eV are scattered up to 2 keV X-rays by electrons with Lorentz factor  $\gamma_x \sim \sqrt{h\nu_x/E_{cmb}} \sim 10^3$ , where  $h$  is the Planck constant. Unless the macroscopic Lorentz factor of the jet is  $\gtrsim 10$ ,  $\gamma_x$ -electrons are non-thermal and follow a power-law energy distribution  $N_e = K_e \gamma^{-p}$ , with  $p = 2\alpha + 1 = 2.5$ . The X-ray specific luminosity can be written as  $L_x \sim N_e(\gamma_x) \gamma_x^3 / t_{ic}(\gamma_x) V_x$ , where  $t_{ic}$  is the IC cooling timescale and  $V_x$  is the volume of the X-ray emitter. From the previous equation we estimate  $K_e$  and therefore, the electron energy density required to explain  $L_x$  is

$$U_e \sim K_e \left( \frac{\gamma_{min}^{2-p}}{p-2} \right) V_x \sim 10^{-9} \left( \frac{\gamma_{min}}{50} \right)^{-0.5} \left( \frac{V_x}{300 \text{ arcsec}^3} \right)^{-1} \text{ erg cm}^{-3}, \quad (1)$$

where  $N_e$  terminates at  $\gamma_{min}$ . The magnetic field in equipartition with non-thermal particles, i.e.  $B_{eq}^2/(8\pi) = (1+a)U_e$ , where  $a$  takes into account the contribution of non-thermal protons, is

$$B_{eq} \sim 160(1+a)^{0.5} \left( \frac{\gamma_{min}}{50} \right)^{-0.25} \left( \frac{V_x}{300 \text{ arcsec}^3} \right)^{-0.5} \mu\text{G}. \quad (2)$$

Note that  $B_{eq} \sim 1.6$  mG if  $a = 100$ . However, the equipartition field is an upper limit, and the magnetic field in  $V_x$  is not necessarily the same as that in the MERLIN emitter, as we will see in the next section.

---

<sup>2</sup>Given that the southern hotspot is located at  $\sim 0.5$  Mpc from the nucleus, absorption of the emission by photoionization is ruled-out (see e.g. Ryter et al. 1996).

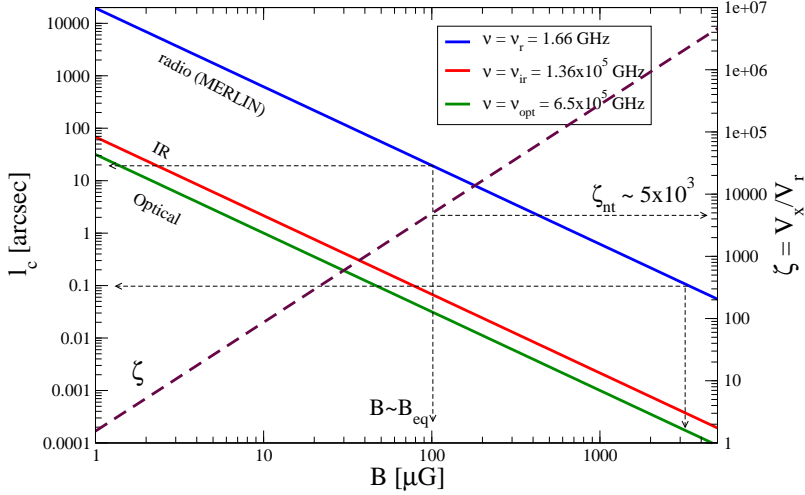


Figure 2. *Left axis* (solid lines): Synchrotron cooling length at radio (1.66 GHz), IR and optical frequencies. *Right axis* (dashed line): X-rays to MERLIN emission volume.

## 2.2. Synchrotron radio emission

The synchrotron emission at  $\nu_r$  is produced by electrons with  $\gamma_r \equiv \gamma(\nu_r) \sim 1.8 \times 10^3 (B/100 \mu\text{G})^{-0.5}$ , where  $\gamma(\nu) \sim 4.5 \times 10^{-4} (\nu/B)^{0.5}$  is the Lorentz factor of electrons emitting synchrotron radiation at frequency  $\nu$  in a magnetic field  $B$ . In a similar way to  $L_x$ , we write  $L_r \sim N_e(\gamma_r) \gamma_r^3 / t_s(\gamma_r) V_r$ , where  $t_s = 7.5 \times 10^{-8} / (B^2 \gamma)$  is the synchrotron cooling timescale and  $V_r$  is the volume of the MERLIN emitter. Therefore,  $L_x/L_r \sim (\gamma_x/\gamma_r)^{3-p} (U_{\text{cmb}}/U_{\text{mag}}) \zeta$ , where  $U_{\text{mag}} = B^2 / (8\pi)$  and  $\zeta \equiv V_x/V_r$ , and we find that

$$\zeta \sim 4.9 \times 10^3 \left( \frac{B}{100 \mu\text{G}} \right)^{1.75}. \quad (3)$$

In Fig. 2 (right axis, dashed line) we can see that  $B \sim B_{\text{eq}}$  corresponds to  $\zeta_{\text{eq}} = 5 \times 10^3$ . Such a large ratio between emitting volumes is not implausible provided the magnetic field is inhomogeneous in the shock downstream region and the synchrotron emitter consists of features smaller than the MERLIN point spread function (FWHM 0.15'') as seen in parts of the MERLIN data. (Note that if  $V_x = V_r$ , a very small magnetic field ( $< \mu\text{G}$ ) would be needed to explain the observed fluxes.) Therefore, X-ray emission is produced in volume  $V_x \gg V_r$ , as we can see in Fig. 1, and the magnetic field in  $V_r$  is much larger than the jet magnetic field of the order of  $\mu\text{G}$  (Hardcastle & Krause 2014). As we will discuss in the following, this may be the result of magnetic field amplification.

### 3. The (synchrotron) hotspot as a magnetic field damping region

The synchrotron ( $l_s$ ) and IC ( $l_{ic}$ ) cooling length of electrons with Lorentz factor  $\gamma$  is  $l_{s,ic}(\gamma) = t_{s,ic}(\gamma)v_{sh}/7$ , where  $v_{sh}/7$  is the velocity of the plasma downstream of the shock. The shock velocity is approximately the same as the jet velocity which we take to be  $v_{sh} = c/3$  (Steenbrugge & Blundell, 2008). We use 7 as the shock compression ratio for a non-relativistic shock whose downstream thermal pressure is dominated by relativistic electrons, although 4 may still apply if non-relativistic ions dominate the pressure downstream of the shock. Our conclusions are not sensitive to the exact value of the shock compression ratio.

#### 3.1. X-ray emitter determined by adiabatic expansion

The IC cooling length of X-ray emitting electrons is  $l_{ic}(\gamma_x) \sim 10^4(3v_{sh}/c)$  arcsec, much larger than  $l_x$ , and therefore IC emission is not the mechanism that determines the size of X-ray emitter. The synchrotron cooling length  $l_s$  of  $\gamma_x$ -electrons is also greater than  $l_x$ , unless the magnetic field in the X-ray emitting region is  $\sim 360 \mu\text{G}$ , greater than  $B_{eq}$  (unless  $V_x \sim 60 \text{ arcsec}^3$ ). However, such a large value of  $B$  in  $V_x$  would produce a synchrotron flux much greater than that detected by the Very Large Array in the A-configuration (Erlund et al. 2007). Therefore, adiabatic expansion is probably the dominant cooling mechanism as the particles flow out of the hotspot.

#### 3.2. MERLIN emitter determined by magnetic field damping

The cooling length of electrons emitting synchrotron radiation at frequency  $\nu$  in a magnetic field  $B$  is

$$\frac{l_s(\nu)}{[\nu]} \sim 12 \left( \frac{\nu}{\text{GHz}} \right)^{-0.5} \left( \frac{B}{100 \mu\text{G}} \right)^{-1.5} \left( \frac{v_{sh}}{c/3} \right). \quad (4)$$

In the Fig. 2 (left axis, solid lines) we plot  $l_s(\nu_r)$ ,  $l_s(\nu_{ir})$  and  $l_s(\nu_{opt})$ . Optical and IR emission are almost co-spatial, with  $l_s(\nu_{ir}) \sim l_s(\nu_{opt}) \sim 0.03''(B/100 \mu\text{G})^{-1.5}(3v_{sh}/c)$  and indicating that these particles radiate most of their energy within  $l_r$ <sup>3</sup>. On the other hand, the synchrotron cooling length of MERLIN emitting electrons is  $l_s(\nu_r) \sim 9.3''(B/100 \mu\text{G})^{-1.5}(3v_{sh}/c) \gg l_r$ . Even worse, the real hotspot extent downstream of the shock is  $L < l_r$  if the jet is lying at an angle  $\theta_j < 90^\circ$  with the line of sight. In particular,  $L = (l_r - D \cos \theta_j) / \sin \theta_j \sim 0.1''$  when the hotspot is modelled as a cylinder of width  $L$  and diameter  $D = 3''$ , and  $\theta_j = 73^\circ$  and  $l_r \sim 1''$  (see the right panel of Fig. 1). In such a case, a very large magnetic field  $B_{cool} \sim 2.4(3v_{sh}/c)^{2/3} \text{ mG}$  would be required to match  $l_s(\nu_r) = 0.1''$ . This value is greater than  $B_{eq}$  for a wide range of  $\gamma_{min}$ - and  $V_x$ -values, suggesting that the downstream extent of the compact emission detected at  $\nu_r$  is not the result of fast synchrotron cooling. We suggest that the MERLIN emission region is determined by magnetic field amplification, as we explain below.

<sup>3</sup>The diffuse IR and optical emission detected also in hotspots in other sources has been suggested to be the result of reacceleration of non-thermal electrons by second order Fermi acceleration (Brunetti et al. 2003). However, this diffuse emission can be also the result of CMB photons up-scattered by electrons with  $\gamma \sim 50$ , or synchrotron emission of electrons with  $\gamma \sim \gamma_{ir} \sim \gamma_{opt}$  in a region with a smaller magnetic field, outside the MERLIN emitter.

#### 4. Magnetic field amplification in mildly relativistic shocks

Remarkable advances have been made in the last decade concerning DSA in the non- and ultra-relativistic regimes. In the former case, the realisation that Non Resonant Hybrid instabilities (Bell 2004) in supernova remnants are fast enough to amplify (and maintain) the magnetic field by orders of magnitude (Vink & Laming 2003) and accelerate particles up to the knee ( $10^{15.5}$  eV) of the cosmic ray spectrum, has shed light on the origin of Galactic cosmic rays. In the ultra-relativistic case, however, theoretical studies show that Weibel instabilities amplify the magnetic field on a short scale length, producing a rapid decay of the fluctuations and thereby inhibiting particle acceleration to ultra high energies (Sironi *et al.* 2013, Reville & Bell 2014). The mildly relativistic regime has not been well studied (see however Brett *et al.* 2013).

In the present contribution we show a case study where the synchrotron cooling cannot determine the thickness of the radio emission detected with the high resolution interreferometer MERLIN. Therefore, we suggest that the magnetic field in the southern arc in 4C 74.26 is amplified since  $B \sim 100 \mu\text{G}$  (required to explain the observations) is much larger than the expected value in the jet upstream of the termination shock (e.g. Hardcastle & Krause 2014). In addition to the thickness of the synchrotron emitter, the cut-off of the synchrotron spectrum can give us an extra (and complementary) piece of evidence that the magnetic field damps near the shock front.

##### 4.1. Synchrotron turnover and magnetic field damping

The synchrotron turnover  $\nu_c$  between  $\nu_{\text{ir}}$  and  $\nu_{\text{opt}}$  indicates that the maximum energy of non-thermal electrons is

$$E_c = \gamma_c m_e c^2 \sim 0.9 \left( \frac{\nu_c}{\nu_{\text{opt}}} \right)^{0.5} \left( \frac{B}{100 \mu\text{G}} \right)^{-0.5} \text{ TeV}, \quad (5)$$

where  $\gamma_c \equiv \gamma_s(\nu_c)$ . The standard assumption is that  $\gamma_c$  is determined by a competition between shock acceleration and synchrotron cooling. By equating  $t_{\text{acc}}(\gamma_c) = t_s(\gamma_c)$ , where  $t_{\text{acc}} \sim 20D/v_{\text{sh}}^2$  is the acceleration timescale for the case of a parallel shock, we find that the electron diffusion coefficient  $D$  is much larger than the Bohm value  $D_{\text{Bohm}}$ :

$$\frac{D}{D_{\text{Bohm}}} \sim 10^6 \left( \frac{v_{\text{sh}}}{c/3} \right)^2 \left( \frac{\nu_c}{\nu_{\text{opt}}} \right)^{-1}, \quad (6)$$

and independent of  $B$ . Such a large diffusion coefficient is allowed if  $B$  is structured on a scale  $s$  much smaller than the Larmor radius of the electrons being accelerated, producing  $D \sim (r_g/s)D_{\text{Bohm}}$  and

$$s \sim 2 \times 10^7 \left( \frac{\nu_c}{\nu_{\text{opt}}} \right)^{1.5} \left( \frac{B}{100 \mu\text{G}} \right)^{-1.5} \left( \frac{v_{\text{sh}}}{c/3} \right)^{-2} \text{ cm}. \quad (7)$$

In comparison the ion skin-depth is  $c/\omega_{\text{pi}} \sim 2.3 \times 10^9 (n/10^{-4} \text{ cm}^{-3})^{-0.5}$  cm, where  $n$  is the particle density downstream of the shock ( $n = 7n_j$ , where the  $n_j$

is the jet density), and

$$\frac{s}{c/\omega_{\text{pi}}} \sim 0.01 \left( \frac{\nu_c}{\nu_{\text{opt}}} \right)^{1.5} \left( \frac{v_{\text{sh}}}{c/3} \right)^{-2} \left( \frac{B}{100 \mu\text{G}} \right)^{-1.5} \left( \frac{n}{10^{-4} \text{cm}^{-3}} \right)^{0.5}. \quad (8)$$

Therefore,

$$B \leq 4.6 \left( \frac{\nu_c}{\nu_{\text{opt}}} \right) \left( \frac{v_{\text{sh}}}{c/3} \right)^{-4/3} \left( \frac{n}{10^{-4} \text{cm}^{-3}} \right)^3 \mu\text{G} \quad (9)$$

is required to satisfy the condition  $s \geq c/\omega_{\text{pi}}$  in the case that  $E_c$  is constrained by synchrotron cooling. Note however that  $B \propto n^3 \propto n_j^3$ . (In our following paper we explore this condition in depth.)

In the case that the magnetic field is amplified by the Weibel instability, small-scale turbulence ( $s \sim c/\omega_{\text{pi}}$ ) scatters non-thermal electrons during DSA (Sironi et al. 2011). The rapid decay of the magnetic field predicted by numerical simulations would account for the cut-off of synchrotron emission in 4C74.26 being far short than the synchrotron cooling distance of radio-emitting electrons ( $l_r \ll l_s(\nu_r)$ ). However, the hotspot magnetic field has to survive over distances  $\sim 0.05$  kpc ( $\sim 0.1''$ ) downstream of the jet reverse shock, which are much longer than those predicted by simulations. The same discrepancy was found in Gamma-Ray Bursts (e.g. Medvedev et al. 2005, Pe'er & Zhang, 2006). Chang et al. (2008) have shown that the magnetic field generated by Weibel instabilities in ultra relativistic plasmas is maintained constant over a distance  $\sim 100 c/\omega_p$  downstream of the shock, and then decays as  $\propto l^{-1}$ , where  $l$  is the distance downstream the shock. (See also Lemoine 2015 for a similar study in the non-linear regime.)

## 5. Conclusions

We model the radio to X-ray emission in the southern hotspot of the FR II radiogalaxy 4C74.26. Our study is based on three key observational features:

1. The MERLIN emission region is too thin to be the result of fast synchrotron cooling.
2. The radio to IR spectrum ( $\alpha = 0.75$ ) is too flat for the emitting volume to be determined by synchrotron cooling through this wavelength range.
3. The turnover of the synchrotron spectrum at IR/optical frequencies requires  $D \gg D_{\text{Bohm}}$  for any reasonable shock velocity.

These three features fit well in a scenario in which the MERLIN radio emission traces out the region where the magnetic field is amplified by plasma instabilities with small length scale. The magnetic field decays quickly behind the shock accounting for the maximum energy of accelerated electrons at  $E_c \sim \text{TeV}$ . These electrons continue up-scattering CMB photons, thus producing IC X-ray emission downstream of the shock after the MERLIN radio emission has ceased.

The magnetic field in equipartition with non-thermal electrons in the MERLIN emission region is  $\sim 100 \mu\text{G}$  and similar to the values obtained by other authors. An unrealistically large magnetic field  $B_{\text{cool}} \sim 2.4 (3v_{\text{sh}}/c)^{2/3} \text{ mG}$  would

be needed to explain the compact radio emission in terms of synchrotron cooling. If  $B \sim 100 \mu\text{G}$  in the synchrotron emission region, the maximum energy of non-thermal electrons is  $\sim \text{TeV}$ , (Eq. 5). If ions are accelerated as well, protons with energy  $\sim \text{TeV}$  diffuse also with  $D \gg D_{\text{Bohm}}$  and then the maximum proton energy at the termination shock of 4C74.26 is only 100 TeV instead of the 100 EeV indicated by the Hillas parameter. This may have important implications for the understanding of the origins of ultra high energy cosmic rays.

**Acknowledgments.** A.T.A. and A.R.B. thank the organisers of the HE-PRO V conference for their kind hospitality. The research leading to this article has received funding from the European Research Council under the European Community's Seventh Framework Programme (FP7/2007-2013)/ERC grant agreement no. 247039. We acknowledge support from the UK Science and Technology Facilities Council under grant No. ST/K00106X/1.

## References

Araudo, A. T., Bell, A. R., Blundell, K. M. 2015, *ApJ*, 806, 243  
 Bell, A. R. 1978, *MNRAS*, 182, 147  
 Bell, A. R. 1978, *MNRAS*, 182, 444  
 Bell, A. R. 2004, *MNRAS*, 353, 550  
 Bret, A., Stockem, A., Fiuzza, F., Ruyer, C., Gremillet, L., Narayan, R., Silva, L.O. 2013, *Physics of Plasmas*, 20, 042102  
 Brunetti, G.; Mack, K.-H.; Prieto, M. A.; Varano, S. 2003, *MNRAS*, 345, 40L  
 Chang, P., Spitkovsky, A., Arons, J. 2008, *ApJ*, 374, 378  
 Erlund, M. C., Fabian, A. C., Blundell, K. M., Moss, C., Ballantyne, D. R. 2007, *MNRAS*, 379, 498  
 Erlund, M. C., Fabian, A. C., Blundell, K. M., Crawford, C. S., Hirst, P. 2010, *MNRAS*, 404, 629  
 Hardcastle, M. J.; Harris, D. E.; Worrall, D. M.; Birkinshaw, M. 2004, *MNRAS*, 612, 729  
 Hardcastle, M. J., Krause, M.G.H. 2014, *MNRAS*, 443, 1482  
 Lemoine, M. 2015, *Journal of Plasma Physics*, 81, 455810101  
 Meisenheimer, K., Roser, H.-J., Hiltner, P. R., Yates, M. G., Longair, M. S., Chini, R., Perley, R. A. 1989, *A&A*, 219, 63  
 Pe'er, A., Zhang, B. 2006, *ApJ*, 653, 454  
 Reville, B., Bell, A. R. 2014, *MNRAS*, 439, 2050  
 Ryter, Ch. E. 1996, *Ap&SS*, 236, 285  
 Sironi, L., Spitkovsky, A. 2011, *ApJ*, 726, 75  
 Sironi, L., Spitkovsky, A., Arons J. 2013, *ApJ*, 771, 54  
 Steenbrugge, K. C., Blundell, K. M. 2008, *MNRAS*, 388, 1457  
 Vink, J., Laming, J.M. 2003, *ApJ*, 554, 758  
 Werner, M. W., Murphy, D. W., Livingston, J. H., Gorjian, V., Jones, D. L.; Meier, D. L.; Lawrence, C. R. 2012, *ApJ*, 759, 86